Thin–Walled Structures 219 (2026) 114169

Contents lists available at ScienceDirect

Thin-Walled Structures

journal homepage: www.elsevier.com/locate/tws

Full length article

Exploring the role of stochasticity in lattice structures for crush energy absorption capabilities

Leidong Xu [a,1], Filip Penda [a,1], Zumrat Usmanova [b,1], Wei Li [b], Royal C. Ihuaenyi [b], Juner Zhu [b,*], Ruobing Bai [b,*], Hongyi Xu [a,*]

[a] School of Mechanical, Aerospace, and Manufacturing Engineering, University of Connecticut, Storrs, CT, 06269, United States
[b] Department of Mechanical and Industrial Engineering, Northeastern, University, Boston, MA, 02115, United States

ARTICLE INFO

Keywords:
Stochasticity
Lattice structures
Crush energy absorption
Stiffness
Weight

SUMMARY

This work presents a systematic study of the relationship between structural stochasticity and the crush energy absorption capability of lattice structures, with controlled stiffness and weight. We develop a Voronoi tessellation-based approach to generate multiple series of lattice structures with either equal weight or equal stiffness, smoothly transitioning from periodic to stochastic configurations for crush energy absorption analysis. The generated lattice series fall into two categories, originating from periodic honeycomb and diamond lattice structures. A new stochasticity metric is proposed for quantifying the structural stochasticity and is compared with the state-of-the-art stochasticity metrics to ensure a consistent measurement. The crush energy absorption properties are obtained using explicit finite element analysis and we observe similar stochasticity-property trends in simulations using both elastic-plastic and hyperelastic materials. We report a new observation that an intermediate level of stochasticity between periodic and high randomness leads to the best crush energy absorption performance. Our analysis reveals that this optimal performance arises from enhanced activation of deformation hinges, promoting efficient energy absorption.

1. Introduction

Recent advances in manufacturing have significantly enhanced the precision of fabricated structural geometries, enabling the fabrication of highly complex designs [1–5]. Concurrently, these advancements have facilitated the application of various established structural optimization methods, such as topology optimization [6–8] and machine learning [9–11], to efficiently design metamaterials [12–15] and lattice structures [16–21] for superior performance. Meanwhile, while most existing metamaterial microstructures are designed based on periodic unit cells, stochastic (disordered) microstructures are gaining growing attractions due to their unique characteristics, including lightweight [22], stiffness [23], mechanical resilience [24,25], and programmable mechanics [26,27]. However, the influence of structural randomness on performance metrics related to large deformation, such as the ability of a structure to absorb crush energy and limit peak loads during a collision, remains poorly understood. While most prior studies of energy-absorbing lattices have focused on through-thickness (out-of-plane) crushing of honeycomb-type cores, in-plane compression has also been widely investigated [28,29], including for stochastic and Voronoi-based architectures [30,31]. The in-plane configuration adopted in this study captures the dominant deformation mechanisms relevant to crash energy absorption while allowing efficient, high-throughput comparison across stochasticity levels. This work systematically quantifies how controlled degrees of structural stochasticity affect the crush energy absorption of lattice structures at a constant stiffness or weight. It addresses a critical knowledge gap, unexplored by prior studies that focused only on narrow disorder ranges and reported contradictory trends.

Conversely, comparative studies in literature reveal mixed conclusions regarding stochastic versus periodic lattices. Recent studies indicate that introducing stochasticity to lattice structures can either reduce or enhance certain mechanical performances compared to their periodic counterparts. For example, structural stochasticity has been observed to result in lower stiffness [32], higher tolerance to flaws in the plastic regime [33], lower maximum stress when damages are introduced to the structure [34], and higher strength and energy absorption capability

* Corresponding authors.
E-mail addresses: j.zhu@northeastern.edu (J. Zhu), ru.bai@northeastern.edu (R. Bai), hongyi.3.xu@uconn.edu (H. Xu).
[1] Equal contribution.

https://doi.org/10.1016/j.tws.2025.114169
Received 27 June 2025; Received in revised form 13 October 2025; Accepted 28 October 2025
Available online 29 October 2025

[35]. However, a common limitation of these studies is their focus on a narrow range of stochastic lattice types. This has limited the comprehensive, quantitative understanding of how structural stochasticity influences mechanical performance. An important question remains unanswered: what is the benefit of introducing structural stochasticity (also referred to as structural disorderliness, irregularity, or randomness) in the design of lattice structures?

Prior studies have also investigated the internal quantitative relationship among different aspects of structural stochasticity, measured using stochasticity metrics [26,36–39] and structural mechanical performances [40–52]. Most of these studies generate lattice structures with varying levels of stochasticity by perturbing a honeycomb-type periodic lattice structure (e.g., perturbing locations of cell centers or lattice joint nodes), while maintaining a consistent number of lattice cells, ranging from periodic to highly random. The conclusions of these studies, which sometimes contradict each other, include the following:

- Higher stochasticity leads to lower elastic stiffness [40–44], tensile strength [45,53], and hydrostatic strength [46], but higher plastic collapse strength [42] and plateau crash pressure (better energy absorption capability) [47].
- Higher stochasticity accelerates the stress wave propagation and reduces the plateau crash stress [48].
- A certain moderate level of structural stochasticity leads to the highest strength, energy absorption [49,50], fracture toughness [45,51,52], and plastic-collapse strength [44].

A few exceptions also exist in addition to the aforementioned studies based on honeycomb-type lattice structures with constant numbers of lattice cells. Christodoulou et al. [54] considered both the number of lattice cells and the lattice weight. When the number of lattice cells is kept invariant during structure generation by cell perturbation, the lattice weight may vary significantly due to the variation in the total length of cell edges (i.e., total length of lattice bars). It is reported that higher stochasticity leads to lower elastic stiffness for low-weight lattices but higher elastic stiffness for high-weight lattices. In addition, higher stochasticity reduces the Mode-I toughness. Montiel et al. [55] generated lattice structures with various levels of stochasticity based on triangular, square, and honeycomb initial structures. They also considered both the number of lattice cells and the degree of connection. Their study shows that increasing structural stochasticity leads to lower elastic stiffness in highly connected (triangular) lattices but higher elastic stiffness in weakly connected (honeycomb) lattices. In a later work, Luan et al. [56] reported the same trend in the relationship between nodal connectivity and stiffness.

Apart from the contradictive conclusions of different literature, the benefits of introducing stochasticity into lattice structures remain unclear. By varying the stochasticity of lattice structures, existing studies have provided insights into trade-offs among stiffness, weight, and nonlinear properties such as crash energy absorption. However, the following question remains unanswered: what is the relationship between structural stochasticity and crush energy absorption, while keeping the same stiffness or weight among different stochastic structures? As one of the most fundamental considerations in engineering applications, the answer to this question will directly help to determine how crush energy absorption can be improved without sacrificing stiffness or weight.

This paper addresses the above question by providing insights into the physical mechanism underlying the trends observed. We will numerically study 2D lattice structures with varying levels of stochasticity and quantify the relationship between structural stochasticity and properties such as energy absorption and crash force efficiency. As shown in Fig. 1, this research work includes three stages:

1. **Data Generation and Sample Selection**: We will generate a comprehensive database of lattice structure samples, encompassing a wide range of stochasticity levels. These lattice structures are created using a specialized algorithm that introduces controlled randomness into the geometric arrangement of the lattice elements. Once the database is established, the elastic properties and mass of each structure are evaluated for analysis in the subsequent stages.
2. **Crushing Simulation**: A carefully curated set of samples are selected from the database, ensuring that either stiffness or weight is kept constant while continuously varying the level of stochasticity. Based on these samples, we will investigate the effect of structural stochasticity on crush energy absorption while minimizing the influence

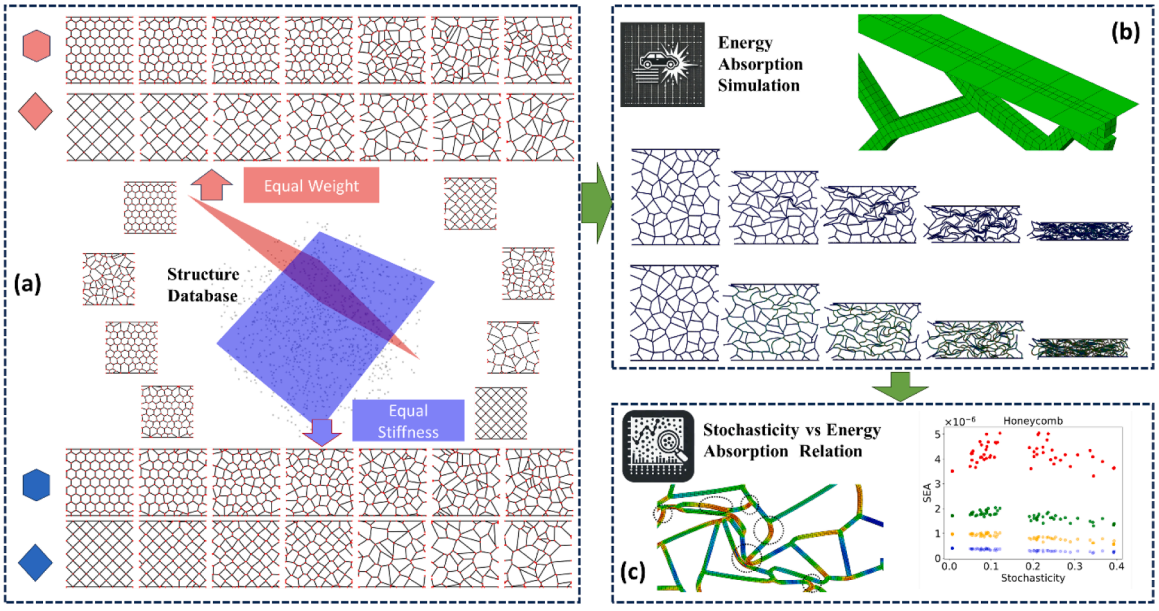

Fig. 1. Schematic overview of the methodology and objectives. (a) A diverse database of lattice structures is created through the controlled generation of lattice architectures with varying weight, stiffness, and levels of structural stochasticity. 40 lattice series with equal stiffness or equal weight are selected. (b) High fidelity structure crush simulations are performed to assess their crush energy absorption properties. (c) Data analysis is performed to unveil the relationship between structural stochasticity and crush energy absorption properties.

of other factors. The selected samples are subjected to crushing simulations using finite element analysis (FEA) under 2D compressive loading conditions until a specified deformation level is reached. These simulations capture the complex interactions between lattice elements during crushing, including progressive failures and energy absorption. Key metrics such as force-displacement curves, specific energy absorption (SEA), and crash force efficiency (CFE) are recorded throughout the simulations. These metrics offer valuable insights into the performance of the lattice structures under crushing loads, serving as the foundation for subsequent analysis.

3. **Data Analysis**: In the final stage, we will analyze the extracted key metrics from simulation data and establish their relationships with the level of structural stochasticity. A discussion of the underlying mechanisms is also provided.

2. Methodology

2.1. Lattice structure database generation

A comprehensive database of lattice structures is generated to

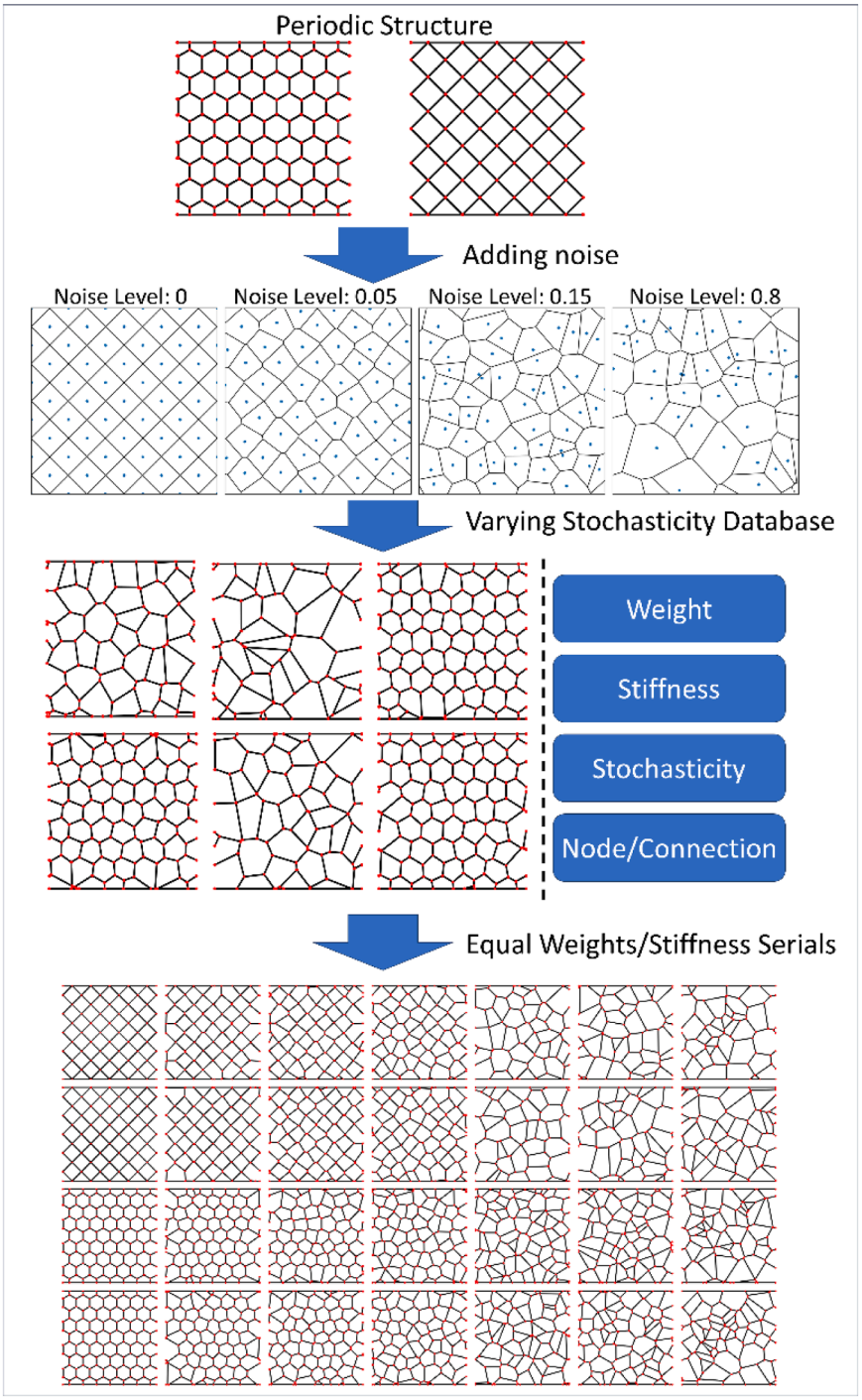

Fig. 2. Top: Overview of the lattice generation process for database construction. Starting from simple periodic designs (top), controlled perturbations are introduced to produce a database of Voronoi-based lattice structures with varying levels of stochasticity. Central perturbation and the resulting lattice structures generated by applying uniform noise levels of 0.05, 0.15, and 0.8. The bottom side of the figure shows two serials of equal-weight or equal-stiffness with increasing stochasticity.

systematically explore how varying degrees of stochasticity influence stiffness and crush energy absorption. Starting from baseline periodic designs such as periodic honeycomb and diamond patterns, structural stochasticity is gradually introduced to create lattice ensembles that continuously span from perfectly regular to highly stochastic geometries.

Each lattice structure is treated as a cellular structure, where the boundaries of the cell correspond to the lattice beams, and the interior region of the cell corresponds to voids. Structural stochasticity is introduced by perturbing cell center locations, and, consequently, the cell boundaries through Voronoi tessellation.

Voronoi tessellation is the partitioning of a plane into regions based on a given set of points, called seeds or centers. Each seed corresponds to a region called a Voronoi cell, which consists of all points in the plane that are closer to that seed than to any other seed. The formal definition of a Voronoi cell is

$$R_k = x \in X | d(x, P_k) \leq d(x, P_j), \text{ for all } j \neq k, \tag{1}$$

where R_k represents a specific Voronoi cell in the Voronoi diagram. $x \in X$ means that x is a point in space X, where X is the entire plane or space in which the Voronoi diagram is constructed. $d(x, P_k) \leq d(x, P_j)$ is a condition that compares the distances between the point x and two different seed points (centers) P_k and P_j. To ensure continuity and eliminate edge effects, periodic boundary conditions are applied during the generation of the lattice geometries. Controlled perturbations are applied to the positions of these cell centers, using a Voronoi tessellation approach to define the final lattice architecture.

By varying the magnitude of perturbation, we produce families of lattices with varying stochasticity levels (irregularities). The effect of the perturbation magnitude is shown in Fig. 2. In practice, we perturb the coordinates of the cell centers of the periodic structure using a displacement from an unbiased uniform distribution bounded by $\pm b$. We sweep sixteen levels, b = 0.01, 0.02, 0.03, 0.04, 0.05, 0.06, 0.07, 0.08, 0.09, 0.10, 0.12, 0.14, 0.16, 0.18, 0.25, 0.30, and for each level generate 500 independent realizations per topology using the same perturbation rule, which results in 8000 stochastic lattice samples. In addition to varying the perturbation magnitude, for each topology we also consider three baseline cell sizes, defined as three center-to-center distances for the perfect honeycomb and diamond configurations.

2.2. Crush energy absorption metrics

A widely applied metric for crush energy absorption is the Specific Energy Absorption (SEA) [57,58], which measures the amount of energy absorbed per unit weight of a structure (Fig. 3 left). SEA is mathematically defined as

$$SEA_{weight} = \int \frac{F(\varepsilon) d\varepsilon}{m}, \tag{2}$$

where $F(\varepsilon)$ is the force as a function of compressive strain ε, and m is the mass of the lattice structure.

Since the simulated structures are represented as 2D line networks, and the material density and the cross-sectional area of the beams are constant in the comparative study, the total mass m is proportional to the total length of all beams in the lattice structure. Accordingly, the SEA is normalized by the total beam length rather than by mass as

$$SEA = \int \frac{F(\varepsilon) d\varepsilon}{\sum_{i=1}^{E} L_{e_i}}, \tag{3}$$

where L_{e_i} represents the length of each beam. This 2D normalization (SEA, in mJ/mm) provides a consistent basis for comparison among samples. For reference, using a representative cross-sectional area of 6.4 $\times 10^{-5}$ mm^2 and proposed material properties from Table 2, the reported SEA values can be converted to SEA_{weight} expressed in J/g by multiplying by 5600.

The second metric used in this work is the Crash Force Efficiency (CFE) [59]. CFE measures how effectively a structure maintains a consistent force during deformation, which is crucial for controlled energy absorption and minimizing peak forces transmitted during a crash (Fig. 3 right). CFE is formulated as

$$CFE = \frac{F_{mean}}{F_{peak}}, \tag{4}$$

where F_{mean} is the mean crushing force and F_{peak} is the peak crushing force, evaluated before the structure enters the densification region.

For both SEA and CFE, higher values indicate better crush energy absorption performances.

2.3. Stochastic metrics and their relationship

Prior studies have proposed various metrics for quantifying structural stochasticity, which are summarized in Table 1. The first three metrics focus on connectivity and spatial arrangement of the lattice cells. The fourth metric, Scaled Standard Deviation of Cell Areas, directly quantifies variations in the size of individual Voronoi cells. Structures with large variations in cell areas typically exhibit a wider spectrum of local deformation modes, potentially affecting overall energy absorption capabilities.

In this work, we adopt the coefficient of variation of cell areas, which is mathematically equivalent to the scaled standard deviation of Voronoi cell areas, providing a normalized measure of spatial irregularity. as our primary stochasticity measure and benchmark this metric against other established metrics to ensure consistency in assessing the level of structural stochasticity. We analyze one series of lattice structures with increasing magnitude of perturbation (refer to the lattice structure generation method in Section 2.1) and evaluate the stochasticity metric values for all samples (Fig. 4). Although each metric is derived from a distinct aspect of the geometry such as cell connectivity, spacing regularity, or cell size variability, they exhibit strong correlation. Structures featuring significant irregularities in cell area also display heightened fluctuations in cell-to-cell spacing and local neighbor counts. Such cross-metric consistency indicates that choosing different structural

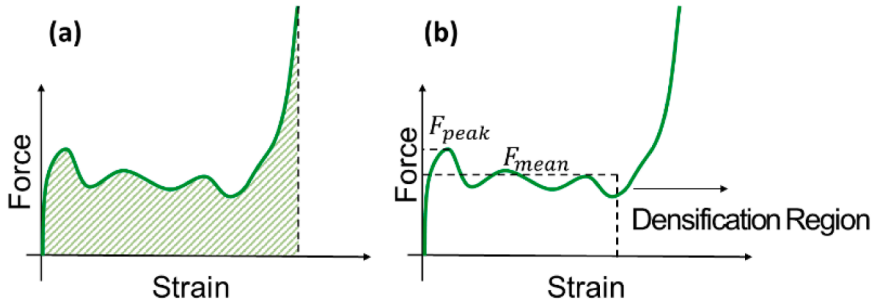

Fig. 3. Visualization of crush energy absorption metric. The x-axis is compressive strain; the y-axis shows (a) SEA and (b) CFE.

Table 1
Summary of stochasticity metrics.

Stochasticity Metric	Mathematical Expression	Property of Interest
Variance of the Number of Neighboring Cells, σ_N^2	$\sigma_N^2 = \frac{1}{M}\sum_{i=1}^{M}(N_i - \mu_N)^2$ $\mu_N = \frac{1}{n}\sum_{i=1}^{n} N_i$ N_i: Number of neighbors of the i th Voronoi cell μ_N: Mean number of neighbors n: Total number of cells	Fracture paths [52]
Variance of the Distance Between Neighbor Cell Nuclei, σ_D^2	$\sigma_D^2 = \frac{1}{m}\sum_{k=1}^{m}(D_k - \mu_D)^2$ $\mu_D = \frac{1}{m}\sum_{k=1}^{m} D_k$ D_k: Distance between the k-th pair of neighboring nuclei μ_D: Mean distance between neighbor nuclei m: Total number of neighboring pairs	Fracture paths [52]
Normalized Minimum Distance Between Neighbor Cell Nuclei δ	$\delta = \frac{\frac{1}{n}\sum_{i=1}^{n} D_{i,\min}}{\mu_D}$ $D_{i,\min}$: Minimum distance between the nucleus of cell i and its neighbors μ_D: Mean distance between neighbor nuclei (from Metric 2) n: Total number of cells	Fracture toughness [49], tensile strength [45], crack toughening [45], elastic moduli [40]
STD of Cell Areas Scaled by the Number of Cells, $\tilde{\sigma}_A$ (proposed in this work; equivalent to CV of cell areas)	$\tilde{\sigma}_A = n\sigma_A = \frac{\sigma_A}{\mu_A}$, *if* $\sum_{i=1}^{n} A_i = 1$ $\sigma_A = \sqrt{\frac{1}{n}\sum_{i=1}^{n}(A_i - \mu_A)^2}$ $\mu_A = \frac{1}{n}\sum_{i=1}^{n} A_i$ A_i: Area of the i th Voronoi cell μ_A: Mean cell area σ_A: Standard deviation of cell areas n: Total number of cells	Energy absorption

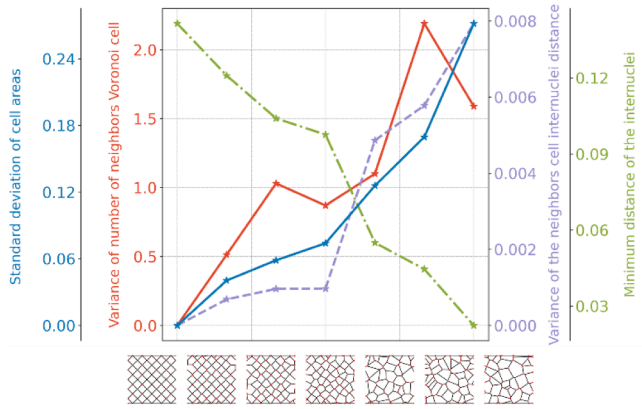

Fig. 4. Comparison of stochasticity metrics for a series of equal-stiffness structures.

stochasticity metrics will not change the final conclusion regarding the structural stochasticity-property relationship. It is important to note that cells adjacent to the domain boundaries are excluded from the stochasticity evaluation to minimize boundary artifacts and obtain more representative results.

To further interpret this metric across the dataset of 16,000 lattice structures, we used the 50th percentile (median) value of 0.234 as the threshold separating moderate and high stochasticity levels. A lower bound of 0.01 was also applied to define the periodic limit, ensuring that minor numerical perturbations near zero were not misclassified as stochastic variations.

2.4. Simulation of structural stiffness and crush energy absorption

Stiffness Characterization Simulation: To determine the elastic stiffness of each lattice structure, we first conduct quasi-static tensile tests using Abaqus/Standard (Implicit). Each generated lattice configuration is discretized using Timoshenko beam elements (B21), which are two-dimensional beam elements incorporating shear deformation effects. The simulations are performed within the linear elastic regime, employing a relatively infinitesimal strain increment of approximately 0.01 %. From the resulting stress-strain curves, we extract the slope in the linear region to obtain the stiffness of each structure.

Crushing Simulation: The crushing response of selected lattice samples is investigated using Abaqus/Explicit. In this stage, the lattices, originally scaled to an effective length of 1 mm, are discretized into three-dimensional, reduced-integration brick elements (C3D8R). To simulate compressive loading, the lattice is placed between two rigid plates. The lower plate is fully fixed, while the upper plate is driven downward to impose compressive deformation. This loading results in up to 80 % strain, applied at quasi-static strain rate of approximately $7s^{-1}$, ensuring negligible inertial effects. To prevent out-of-plane deformation and potential buckling, the lattices are constrained to remain in the XY plane. The reaction force measured at the reference point of the top plate provides the force-displacement data necessary for evaluating the crush energy absorption metrics. Fig. 5(b) presents a comparison between beam and brick elements, and Fig. 5(c) illustrates a comparison between elastic-plastic and hyperelastic materials under varying strain levels. Experimental validation of the simulation model is provided in the Supplemental Information.

Two material models are investigated in this study. The first is an elastic-plastic model for an aluminum alloy (Al-6101 T6) and the second is a hyperelastic model for an elastomer [60]. The specific material properties are provided in Table 2. The Ogden-based hyperelastic model employed in these simulations is characterized by a set of material constants in the following constitutive model:

$$U = \sum_{i=1}^{N} \frac{2\,\mu_i}{\alpha_i^2}\left(\bar{\lambda}_1^{\alpha_i} + \bar{\lambda}_2^{\alpha_i} + \bar{\lambda}_3^{\alpha_i} - 3\right)^i + \sum_{i=1}^{N} \frac{1}{D_i}\left(J^{el} - 1\right)^{2i}, \tag{5}$$

Where $\bar{\lambda}_i$ are the deviatoric principal stretches, N is the number of terms in the summation series, μ_i, α_i, and D_i are material constants, and

Table 2
Representative mechanical properties of the elastic-plastic material model (Al-6101 T6) and parameters for the Ogden-based hyperelastic material model used in the simulation, including shear-like moduli ($\boldsymbol{\mu}_1, \boldsymbol{\mu}_2$), nonlinear exponents ($\boldsymbol{\alpha}_1$, $\boldsymbol{\alpha}_2$), volumetric compressibility parameters ($\boldsymbol{D}_1$, $\boldsymbol{D}_2$), and material density.

Elastic-plastic Material Model	
Property	**Value**
Density	2.79 g/cm^3
Elastic	
Young's Modulus (E)	68,900 MPa
Poisson's Ratio	0.33
Plastic	
Yield Strength	193 MPa
Ultimate Tensile Strength	221 MPa
Plastic Strain	0.17
Hyperelastic Material Model	
μ_1	0.4055 MPa
α_1	2.4580
D_1	6.1616E-3 MPa^{-1}
μ_2	6.1298 MPa
α_2	−1.9004
D_2	0 MPa^{-1}
Density	1 g/cm^3

J^{el} is the elastic volume ratio.

2.5. Generated lattice series of equal stiffness or equal weight

A major contribution of this work is the isolation of two factors, weight and stiffness, in investigating the relationship between structural stochasticity and large deformation behaviors during structure crushing. Weight defines the total amount of material in a structure and stiffness (Young's modulus) determines the linear elastic response of the structure. The elastic properties of each lattice sample are determined through stiffness characterization simulations, while the weight is estimated by summing the lengths of the beams, given that all beams have the same diameter.

Selecting from the large lattice structure database, we obtain 10 series of structures with nearly identical weight (within 1 % error) and another 10 series with nearly identical stiffness (also within 1 % error) relative to the baseline periodic honeycomb and diamond lattices. Each of these series includes 7 structures and spans a broad range of stochasticity, measured by the variation in cell areas. As illustrated in Section 2.3, a stochasticity metric of zero indicates that all Voronoi cells have nearly identical areas, corresponding to two periodic arrangements. As stochasticity increases, the variability in cell sizes grows, leading to more irregular and diverse cell structures.

It is important to note that stochastic structures with identical stiffness or weight as the base structure can be relatively rare at certain levels of stochasticity. Consequently, we identify a total of 230 unique structures from the 8500 lattice samples that meet the equal-stiffness or equal-weight requirements. With these 230 structures, 20 series of lattice structures with increasing stochasticity (ranging from periodic to highly random) are created for the crush energy absorption analysis throughout the remainder of the study. The detailed structures of the 20 series are provided in the supporting materials.

3. Results

3.1. Stochasticity-crush energy absorption relationship: equal stiffness

For elastic-plastic lattices, honeycomb-based and diamond-based lattice series exhibit slightly different trends in the relationship between structural stochasticity and SEA. The honeycomb-based lattices exhibit an increase-decrease trend in SEA with increasing structural stochasticity. The largest SEA is observed at a moderate stochasticity level, though with large sample-to-sample variance. The diamond-based lattices achieve the highest SEA at a low stochasticity level, followed by a decreasing trend in SEA as stochasticity increases. Significant sample-to-sample variations are also observed in the diamond-based lattice series, suggesting that at certain levels of structural stochasticity, individual samples may outperform or underperform the periodic lattice. It also suggests that the benefits of stochasticity in diamond-based lattices are less predictable and may depend more sensitively on the specific structural patterns.

For hyperelastic lattices, honeycomb-based and diamond-based lattice series exhibit similar trends in the relationship between structural stochasticity and SEA. For honeycomb lattices, introducing a certain level of structural stochasticity improves SEA compared to the perfectly periodic structure, albeit with increased sample-to-sample variability. For diamond-based lattices, introducing structural stochasticity induces significantly larger sample-to-sample variations. Some stochastic samples achieve better SEA than the perfectly periodic structure, while others at the same stochasticity level perform worse. This large variance suggests that the benefits of stochasticity in the diamond-based lattices are less predictable and may depend more sensitively on the specific structural patterns.

To quantify the robustness of these trends, non-parametric permutation tests and effect size analyses were performed in Supplemental Information. For the equal-stiffness configurations, the moderate stochasticity group exhibits statistically significant improvement in SEA ($p < 0.05$ in 7–8 of 8 contrasts) with large effect sizes ($\delta \approx 0.7$–0.9). These results confirm that the observed performance enhancement is reproducible and not due to random sampling variations.

If measuring the crush energy absorption using the CFE metric, the periodic honeycomb configuration delivers the highest performance for both elastic-plastic and hyperelastic materials, followed by a general decrease as structural stochasticity increase. The diamond lattices, however, present a more complex trend. When the base material is elastic-plastic, no clear trend is observed. Increasing structural stochasticity can either raise or lower the CFE value, underscoring that the benefit of randomness may be specific configuration-dependent. When the base material is hyperelastic, a decreasing trend is observed as stochasticity increases. The relationship between stochasticity and SEA/CFE under equal-stiffness conditions is illustrated in Fig. 6.

To summarize, when stiffness is held constant, increasing structural stochasticity of the diamond-based lattice to a certain level can achieve the highest crush energy absorption performances, measured by either SEA or CFE. Meanwhile, it is observed that highly stochastic structures do not yield the best performance. Increasing structural stochasticity of the honeycomb-based lattice to a moderate level result in the highest SEA value. However, the overall trend of CFE decreases as stochasticity increases. This finding holds for both elastic-plastic and hyperelastic base material properties.

3.2. Stochasticity-crush energy absorption relationship: equal weight

For elastic-plastic lattices, introducing structural stochasticity to honeycomb-based lattices leads to improvement in SEA, as well as large sample-to-sample variations. Introducing structural stochasticity to diamond-based lattices leads to a generally upward trend in SEA, but with significant sample-to-sample variances. As a result, certain stochastic configurations outperform the periodic reference structure, whereas others fall below. For both honeycomb-based and diamond-based series, samples with the highest SEA are observed at moderate levels of stochasticity.

For hyperelastic lattices, the honeycomb lattices exhibit a more complex stochasticity-SEA relationship. Although an initial increase in SEA is observed at low stochasticity levels, a general downward trend in SEA emerges as stochasticity increases. At high compressive strain (80 %), the large sample-to-sample variance in SEA obscures any clear pattern, indicating that increasing structural stochasticity can either increase or decrease SEA, depending on specific structural patterns. The diamond-based lattices also exhibit significant sample-to-sample variance as structural stochasticity increases. The statistical analysis also confirms that the performance advantage of moderate stochasticity diminishes under the equal-weight constraint. Only a few contrasts achieve statistical significance ($p < 0.05$), and the corresponding effect sizes are smaller ($\delta \approx 0.3$–0.5), indicating a weaker but still measurable improvement. However, a general trend emerges, with peak SEA values observed at moderate levels of stochasticity.

When measuring crush energy absorption using the CFE metric, the periodic honeycomb configuration delivers the highest performance for both elastic-plastic and hyperelastic materials, followed by a general decrease as structural stochasticity increase. On the other hand, in the diamond-based lattices, the highest and the lowest CFE values are achieved at moderate structural stochasticity levels. The relationship between stochasticity and SEA/CFE under equal-weight conditions is illustrated in Fig. 7.

In summary, we observe the same trend in the equal weight case as in the equal stiffness case. Increasing structural stochasticity of the diamond-based lattice to a certain level can achieve the highest crush energy absorption performance, measured by either SEA or CFE, while highly stochastic structures do not yield the best performance. Increasing the structural stochasticity of the honeycomb-based lattice to

a moderate level results in the highest SEA value. However, the overall trend of CFE decreases as stochasticity increases. This finding holds for both elastic-plastic and hyperelastic base material properties.

3.3. Interplay among stiffness, weight, and crush energy absorption

To elucidate the interplay between stiffness, weight, and crush energy absorption metrics, we analyze representative lattice structure samples on Pareto frontiers. These frontiers were identified based on two key crush energy absorption metrics, SEA and CFE, at 80 % strain. Pareto frontier identifies lattice configurations that cannot be improved in one performance metric without sacrificing the other, thus capturing the optimal balance between these competing objectives.

Fig. 8 shows the Pareto frontiers for both honeycomb-based and diamond-based lattices under varying levels of stochasticity. In both types, the Pareto-optimal lattices form a narrow band where moderate levels of stochasticity yield enhanced crush energy absorption performance in both metrics. These findings reinforce our earlier observations: while highly disordered lattices rarely appear along the Pareto frontier, lattices with moderate stochasticity often achieve superior or at least non-inferior trade-offs. This observation suggests that controlled stochasticity may yield lattice architectures that simultaneously excel in both SEA and CFE, offering pathways toward design strategies that balance competing performance goals without compromising stiffness or weight constraints.

4. Discussion and conclusion

Lattice configurations on the Pareto frontier simultaneously achieve high SEA and CFE, illustrating that the interplay between randomization

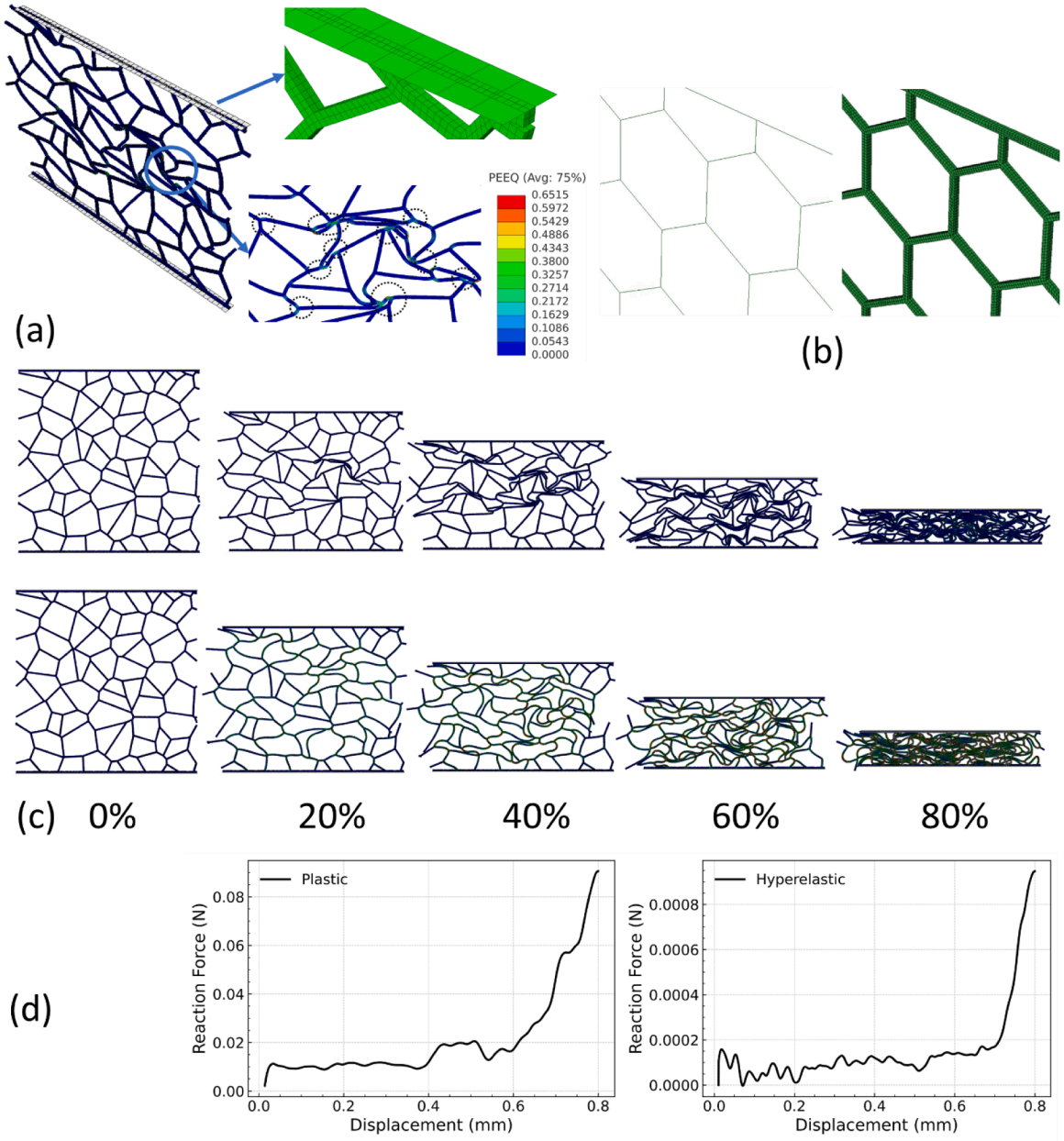

Fig. 5. (a) Representative snapshots of equivalent plastic strain (PEEQ) from the crushing simulations, including an enlarged view of the rigid plate (top) and a close-up of a forming plastic hinge (bottom). (b) A visual comparison of lattice modeling using beam-type B21 elements versus solid-type C3D8R elements. (c) The same lattice structure under various levels of compressive deformation, shown for both elastic-plastic (top series) and hyperelastic (bottom series) material models. (d) Corresponding Reaction force-Displacement curve.

and deformation mechanisms can yield designs that excel both crush energy absorption dimensions. Results presented above demonstrate that controlled degrees of structural stochasticity can significantly influence the crush energy absorption of lattice architectures. Our observations suggest that neither perfectly periodic nor highly disordered configurations yield the best energy absorption performance. Instead, an intermediate level of randomness appears to promote superior crush energy absorption metrics, including both SEA and CFE.

To understand the underlying mechanisms that drive these phenomena, we examine the spatial distribution of deformation, the localization of deformation, and the resulting stress transfer within the lattice. Here, we revisit an important concept of "plastic hinge" that has been extensively used in traditional analysis of structural crashworthiness [61,62]. This concept stemmed from the observation that the large deformation during crash is highly localized in lines that undergo bending, rotating, and folding. The majority of structural energy absorption is through these large-deformation mechanisms around the hinges. Therefore, the number of hinges and the degrees of rotation about them represent the total energy absorption.

Plastic-hinge formation is first extracted for elastic-plastic lattices by scanning the voxel mesh for contiguous clusters in which the element-wise equivalent plastic strain (PEEQ) exceeds 0.1. To filter out numerical noise, a hinge must span at least $2 \times 2 \times 2 = 8$ elements, forming a cube that is two-voxel wide in each direction. This size matches the minimum ligament thickness that can realistically fold in the physical specimens. The PEEQ threshold of 0.1 is physically meaningful. For the elastic-plastic alloy considered, a plastic strain of approximately 10 % marks the onset of significant work-hardening. This strain level also corresponds to the appearance of sharp folds in the simulation snapshots (Fig. 5a). For the hyperelastic lattices that do not exhibit plastic deformation, we define the "hyperelastic hinge" as a cluster with at least $2 \times 2 \times 2 = 8$ elements with elastic strain energy density (ESEDEN) exceeding 0.1. A sensitivity analysis using thresholds between 0.05 and 0.20 show that lower cutoffs tend to overestimate hinge counts. In those cases, the algorithm starts to mislabel diffuse bending regions, where deformation is spread broadly across the lattice rather than being concentrated at a narrow fold. Many elements may exhibit modest strain or energy density, but do not behave like a true hinge that can fold sharply and dissipate energy efficiently. In contrast, thresholds above 0.1 tend to miss actual fold zones. Although PEEQ and ESEDEN track different state variables, their values rise sharply where the lattice stores or dissipates most of the work. Hence plastic hinges in the elastic-plastic model and hyperelastic hinges in the hyperelastic model are mechanically equivalent indicators of the localized folding mechanisms that govern total energy absorbed. An example of the visualization of plastic hinges is shown in Fig. 5(a).

Fig. 9 confirms that the SEA for both diamond and honeycomb lattices scales almost linearly with the total number of hinges that form during progressive collapse. Each additional hinge supplies a comparable increment of dissipated work, so the SEA-hinge count curve mirrors the earlier stochasticity-hinge trend reported in Section 3. By definition, CFE is the ratio of the average reaction force to the peak force, and the hinge count alone provides no information about the geometry or timing of that peak. In other words, knowing how many hinges form does not indicate where and when they nucleate along the loading path. Consequently, two lattices with identical hinge numbers can display very different peak forces (and thus different CFEs), if their hinges nucleate at different locations or stages of collapse.

Figs. S6-S8 at Supporting Information show the evolutions of the strain energy density, displacement contour, and Von Mises stress, respectively, in hyperelastic diamond lattices with various degrees of stochasticity at different compressive strains. At a compressive strain of $\varepsilon = 20$ %, deformation initiates near the top surface with early hinge formation for all degrees of stochasticity. The hinges are more localized in periodic and highly stochastic lattices, but more diffuse in intermediate-stochastic lattices. The number of hinges increases substantially at $\varepsilon = 40$ %. Clusters of hinges emerge in regions with irregular cells in highly stochastic lattices, leading to localized deformation zones and reduced SEA. By contrast, a broader distribution of hinges is observed in intermediate-stochastic lattices, leading to enhanced SEA. At $\varepsilon = 60$ %, hinges become more diffuse across the periodic and intermediate-stochastic lattices, while remaining highly localized in the upper region in highly stochastic lattices.

A similar trend is observed in the strain energy density, displacement

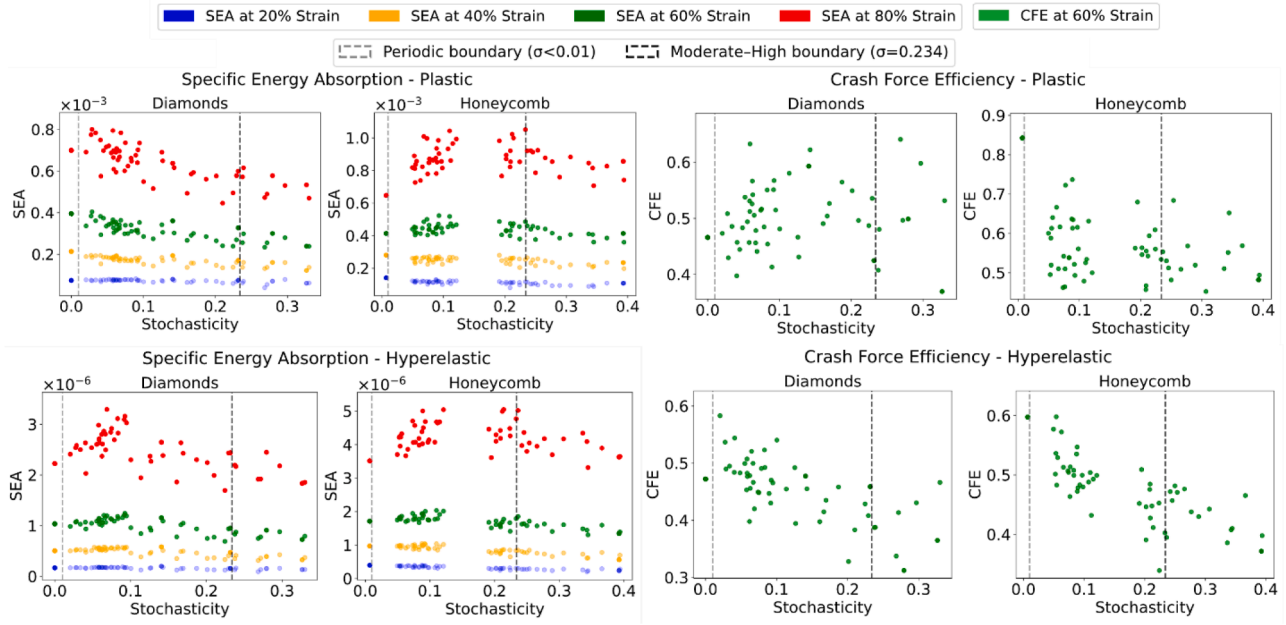

Fig. 6. Influence of stochasticity on crush energy absorption metrics under equal-stiffness conditions. Plots compare SEA in unit length at multiple strain levels (20 %, 40 %, 60 %, and 80 %) and CFE at 60 % strain for both elastic-plastic (top row) and hyperelastic (bottom row) material models in diamond and honeycomb lattices. The percentage of strain represents ratio between the compressed size and original size. Each point represents a distinct lattice configuration with the same stiffness (within a 1 % error margin) but varying degrees of geometric randomness. When the stochastic metric is 0, the structure is periodic.

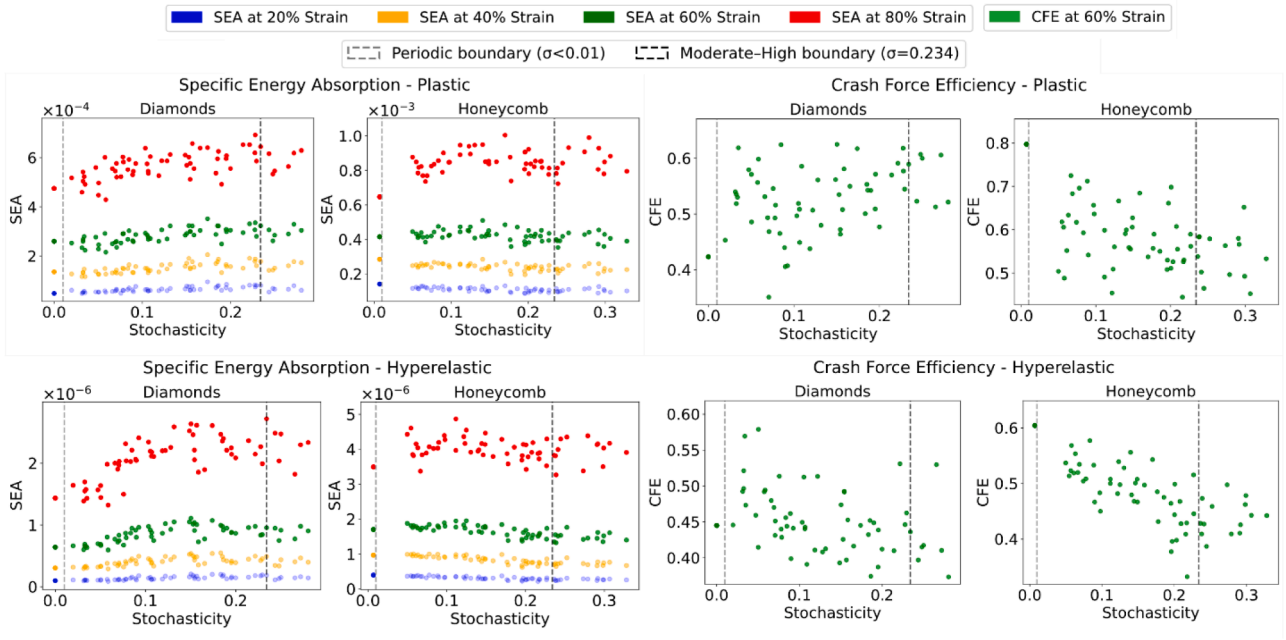

Fig. 7. Influence of stochasticity on crush energy absorption metrics under equal-weight conditions. Plots compare SEA in unit length at multiple compression levels (20 %, 40 %, 60 %, and 80 %) and CFE at 60 % strain for both elastic-plastic (top row) and hyperelastic (bottom row) materials in diamond and honeycomb lattices. The percentage of strain represents ratio between the compressed size and original size. Each point represents a distinct lattice configuration with the same weight (within a 1 % error margin) but varying degrees of geometric randomness.

contour, and Von Mises stress in hyperelastic honeycomb lattices (Figs. S9-S11). With the increase of compressive strain, hinges evolve from initially localized near the top surface to more diffuse at increasing strains. Hinges are also more broadly distributed in periodic and intermediate-stochastic lattices, while more localized in highly stochastic lattices, which agree well with their corresponding SEA performances.

Compared to hyperelastic lattices, plastic lattices with periodic order and intermediate stochasticity show a different initiation of hinges (Figs. S12-S14 for diamond lattices and Figs. S15-S17 for honeycomb lattices): hinges first develop near the mid-plane and progressively diffuse towards the top and bottom with increasing compression. Correspondingly, these hinges are more diffuse and contribute to higher SEA in periodic and intermediate-stochastic lattices. By contrast, hinges are more localized in highly stochastic plastic lattices, similar to their hyperelastic counterparts, leading to lower SEA.

Overall, these observations allude to a generic toughening mechanism for enhanced SEA and CFE in lattices with different cell geometries: an intermediate level of lattice stochasticity leads to a more diffuse distribution of hyperelastic or plastic hinges, hence enhanced SEA and CFE performances. This mechanism is analogous to the well-developed toughening strategy for composites by introducing an intermediate degree of sacrificial bonds breaking for large-scale energy dissipation [63, 64]. Examples include fiber-reinforced composites with an intermediate level of weak fiber-matrix interfaces [65,66], and double-network elastomers or gels with an intermediate amount of physical cross-linkers [67,68].

In summary, moderate stochasticity alters deformation pathways by preventing the formation of a single dominant collapse mode and promoting a more diffuse distribution of hinges and local instabilities. This distributed deformation leads to higher and more stable energy absorption, explaining the superior SEA and CFE observed at intermediate stochasticity levels across both topologies and material models. Moving forward, these insights can guide the development of new design strategies for architected materials, where careful tuning of geometric randomness can yield robust, lightweight structures capable of withstanding extreme loading conditions.

Building on these findings, we will extend the disturbance model beyond the current approach to include a broader range of geometric and manufacturing-relevant perturbations. Future work will explore alternative noise distributions (e.g., Gaussian) and additional disturbance modes such as variations in member dimensions, joint misalignments, and combined perturbations calibrated to realistic manufacturing tolerances. Furthermore, we will investigate the interaction between designed stochasticity and process-induced variability in additive manufacturing (e.g., SLM, DLP), examining whether fabrication errors offset, amplify, or filter the intended randomness. These studies will help establish a process-aware framework linking designed and manufactured stochasticity for improved prediction and robustness of energy-absorbing performance.

CRediT authorship contribution statement

Leidong Xu: Writing – review & editing, Writing – original draft, Visualization, Validation, Software, Methodology, Investigation, Formal analysis, Data curation. **Filip Penda:** Writing – original draft, Visualization, Validation, Software, Methodology, Investigation, Formal analysis, Conceptualization. **Zumrat Usmanova:** Writing – review & editing, Writing – original draft, Visualization, Validation, Software, Methodology, Investigation, Formal analysis, Data curation. **Wei Li:** Writing – review & editing, Writing – original draft, Software. **Royal C. Ihuaenyi:** Writing – review & editing, Investigation. **Juner Zhu:** Writing – review & editing, Writing – original draft, Supervision, Resources, Project administration, Methodology, Funding acquisition, Conceptualization. **Ruobing Bai:** Writing – review & editing, Writing – original draft, Supervision, Resources, Project administration, Methodology, Funding acquisition, Conceptualization. **Hongyi Xu:** Writing – review & editing, Writing – original draft, Supervision, Resources, Project administration, Methodology, Funding acquisition, Conceptualization.

Declaration of competing interest

Hongyi Xu reports financial support was provided by National

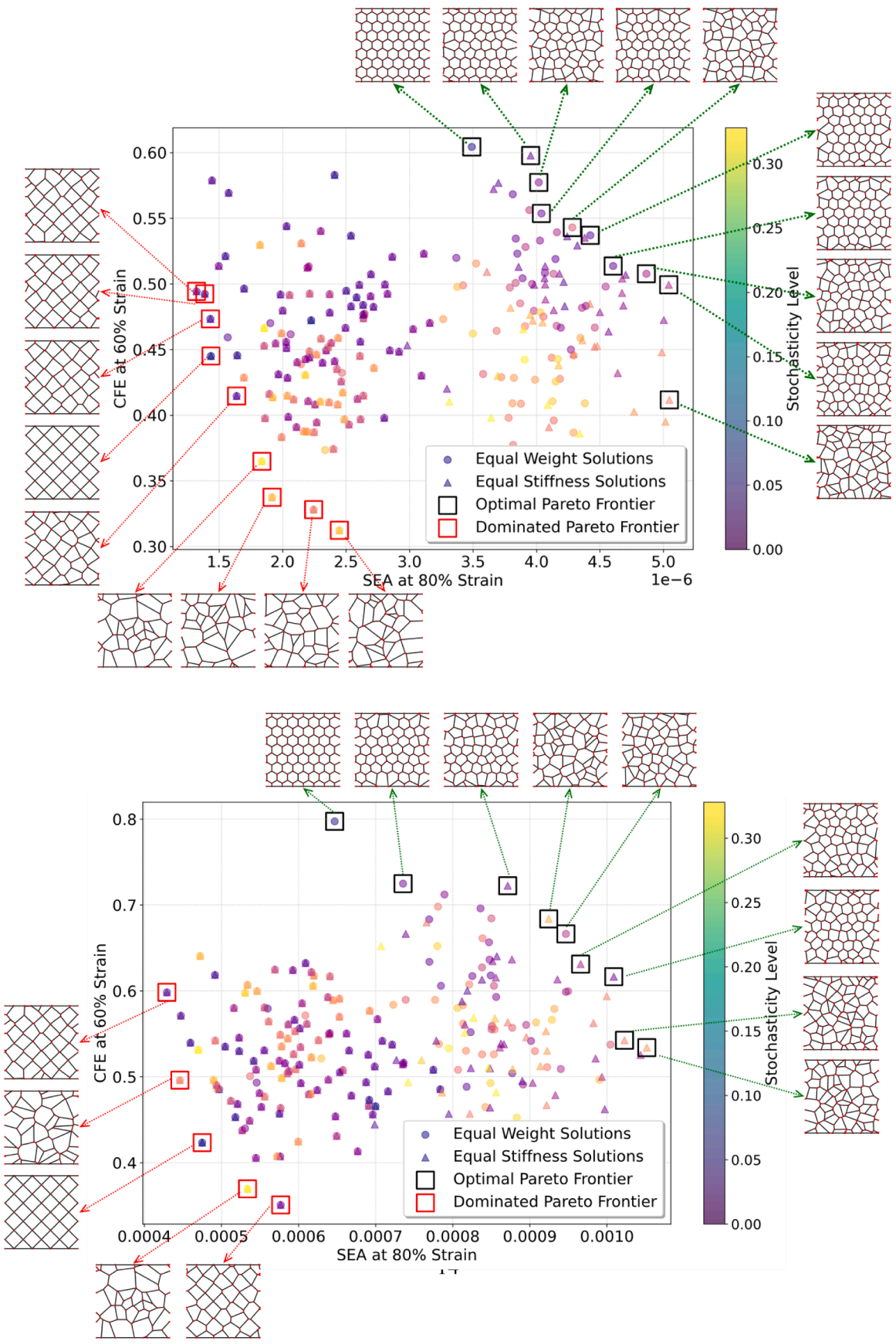

Fig. 8. Pareto frontiers illustrate the trade-off between SEA and CFE at 80 % strain for elastic-plastic (left) and hyperelastic (right) lattice architectures under varying degrees of stochasticity. The optimal pareto sets are highlighted in a black box and the dominated solutions in a red box.

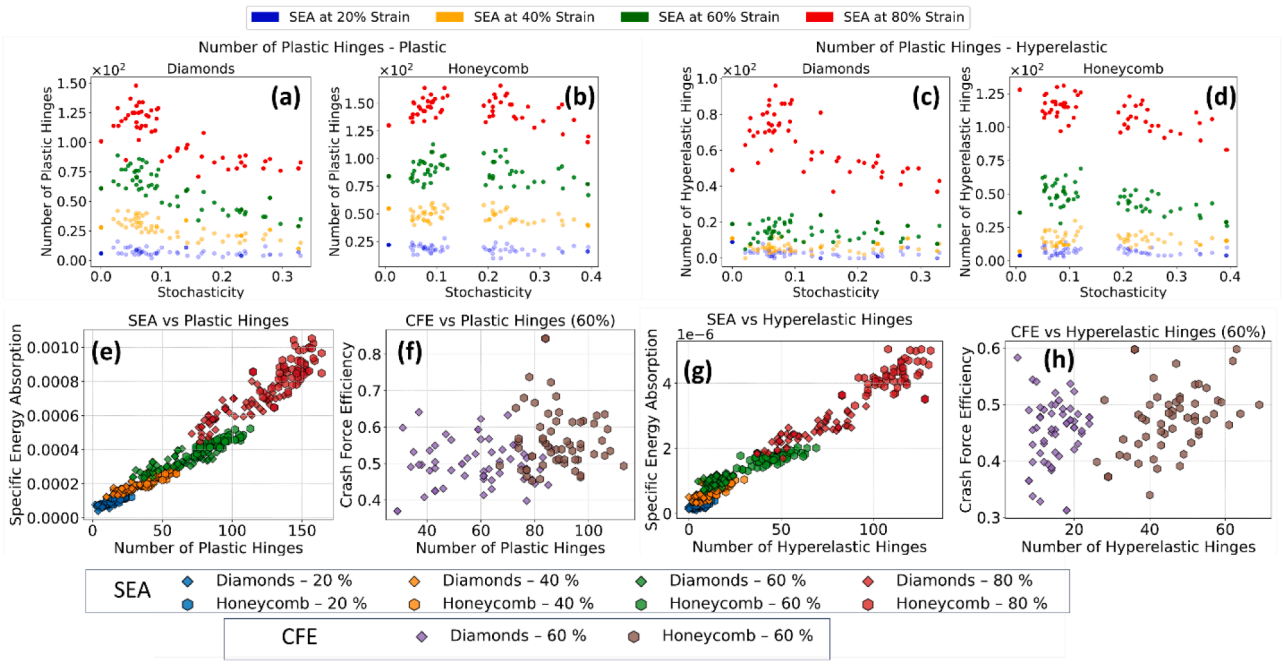

Fig. 9. Top row: number of hinges generated as a function of stochasticity for diamond and honeycomb lattices. (a, b) elastic-plastic material and (c, d) hyperelastic material. Bottom row: Correlation between hinge population and crush energy absorption metrics. (e) Specific energy absorption (SEA) versus total plastic hinge count, (f) CFE at 60 % strain versus plastic hinge count, (g) SEA versus hyperelastic hinge count, and (h) CFE at 60 % strain versus hyperelastic hinge count.

Science Foundation. Ruobing Bai reports financial support was provided by National Science Foundation. Hongyi Xu reports financial support was provided by US Army DEVCOM Ground Vehicle Systems Center. Juner Zhu reports financial support was provided by Ford Motor Company. If there are other authors, they declare that they have no known competing financial interests or personal relationships that could have appeared to influence the work reported in this paper.

Acknowledgement

H.X. and F.P. acknowledge the support under Cooperative Agreement W56HZV-21–2–0001 with the US Army DEVCOM Ground Vehicle Systems Center (GVSC), through the Virtual Prototyping of Autonomy Enabled Ground Systems (VIPR-GS) program. H.X. and L.X. are supported by the National Science Foundation grant CMMI-2142290. Z.U. and R.B. are supported by the National Science Foundation through grant CMMI-2440758. W.L. and J.Z. are supported by Ford Motor Company through a University Research Project. DISTRIBUTION STATEMENT A. Approved for public release; distribution is unlimited. OPSEC9818.

Supplementary materials

Supplementary material associated with this article can be found, in the online version, at doi:10.1016/j.tws.2025.114169.

Data availability

Data will be made available on request.

References

[1] M. Askari, et al., Additive manufacturing of metamaterials: a review, Addit. Manuf. 36 (2020) 101562.
[2] A. Nazir, et al., Multi-material additive manufacturing: a systematic review of design, properties, applications, challenges, and 3D printing of materials and cellular metamaterials, Mater. Des. 226 (2023) 111661.
[3] D. Chen, X. Zheng, Multi-material additive manufacturing of metamaterials with giant, tailorable negative Poisson's ratios, Sci. Rep. 8 (1) (2018) 1–8.
[4] A. Kumar, et al., Design and additive manufacturing of closed cells from supportless lattice structure, Addit. Manuf. 33 (2020) 101168.
[5] X. Cao, et al., Improving predictability of additively manufactured Ti-6Al-4 V lattices for orthopaedic devices: a parametric and struts angle study, Mater. Des. 243 (2024) 113043.
[6] D.O. Cohen, et al., Computational design of additively manufactured curvilinear scaffolds for bone repair with analytical sensitivities, J. Mech. Des. 147 (3) (2025).
[7] L. Liao, et al., Topology optimization design of multi-material coated phononic crystals with load-bearing performance and ultra-wide band gap, Thin Walled Struct. (2025) 113386.
[8] H. Zhengtong, et al., High stable auxetic metamaterials developed through feature-control topology optimization and additive manufacturing, Thin Walled Struct. 213 (2025) 113305.
[9] C. Chu, et al., Exploring VAE-driven implicit parametric unit cells for multiscale topology optimization, Mater. Des. 244 (2024) 113087.
[10] A.E. Gongora, et al., Designing lattices for impact protection using transfer learning, Matter 5 (9) (2022) 2829–2846.
[11] N. YÜKSEL, et al., Mechanical properties of additively manufactured lattice structures designed by deep learning, Thin Walled Struct. 196 (2024) 111475.
[12] D. Lee, et al., t-metaset: task-aware acquisition of metamaterial datasets through diversity-based active learning, J. Mech. Des. 145 (3) (2023) 031704.
[13] Z. Wang, et al., Designing connectivity-guaranteed porous metamaterial units using generative graph neural networks, J. Mech. Des. 147 (2) (2025).
[14] D. Han, et al., Design, fabrication and mechanical properties of a new cylindrical lattice metamaterial, Thin Walled Struct. 213 (2025) 113292.
[15] R. Lu, et al., Quasi-static crushing response of a novel triaxial isotropy mechanical metamaterial with dual-platform property, Thin Walled Struct. 206 (2025) 112630.
[16] H. Kazemi, A. Vaziri, J.A. Norato, Multi-material topology optimization of lattice structures using geometry projection, Comput. Methods Appl. Mech. Eng. 363 (2020) 112895.
[17] H. Jia, et al., Homogenization-based topology optimization for self-supporting additive-manufactured lattice-infilled structure, Mater. Des. 245 (2024) 113264.
[18] Z. Yu, et al., Current research status on advanced lattice structures for impact and energy absorption applications: a systematic review, Thin Walled Struct. (2025) 113490.
[19] Z. Xie, et al., Ballistic performance of additive manufacturing metal lattice structures, Thin Walled Struct. 208 (2025) 112763.
[20] H. Liu, et al., Enhanced mechanical responses and fatigue behaviors of triply periodic minimal surface lattice metamaterials by twin-oriented lattice design, Int. J. Fatigue (2025) 109172.
[21] S. Stammkötter, et al., Fatigue assessment and damage evolution of additively manufactured Ti–6Al–4V lattice structures for medical applications, J. Mater. Res. Technol. 36 (2025) 3007–3014.
[22] F.V. Senhora, E.D. Sanders, G.H. Paulino, Optimally-tailored spinodal architected materials for multiscale design and manufacturing, Adv. Mater. 34 (26) (2022) 2109304.

[23] L. Xu, K.N. Khanghah, H. Xu, Designing mixed-category stochastic microstructures by deep generative model-based and curvature functional-based methods, J. Mech. Des. 146 (4) (2024).
[24] P. Thakolkaran, et al., Experiment-informed finite-strain inverse design of spinodal metamaterials, Extreme Mech. Lett. 74 (2025) 102274.
[25] Y. Guo, S. Sharma, S. Kumar, Inverse designing surface curvatures by deep learning, Adv. Intell. Syst. (2024) 2300789.
[26] C. Sirote-Katz, et al., Emergent disorder and mechanical memory in periodic metamaterials, Nat. Commun. 15 (1) (2024) 4008.
[27] D.R. Reid, et al., Auxetic metamaterials from disordered networks, Proc. Natl. Acad. Sci. 115 (7) (2018) E1384–E1390, p.
[28] J. Fang, et al., On hierarchical honeycombs under out-of-plane crushing, Int. J. Solids. Struct. 135 (2018) 1–13.
[29] G. Sun, et al., Crashworthiness of vertex based hierarchical honeycombs in out-of-plane impact, Mater. Des. 110 (2016) 705–719.
[30] S.D. Papka, S. Kyriakides, In-plane compressive response and crushing of honeycomb, J. Mech. Phys. Solids. 42 (10) (1994) 1499–1532.
[31] A.M.R.M. Ahmed, et al., Mechanical and energy absorption properties of 3D-printed honeycomb structures with Voronoi tessellations, Front. Mech. Eng. 9 (2023) 1204893.
[32] M.J. Silva, L.J. Gibson, The effects of non-periodic microstructure and defects on the compressive strength of two-dimensional cellular solids, Int. J. Mech. Sci. 39 (5) (1997) 549–563.
[33] W. Chen, et al., *Flaw tolerance* vs. *performance: a tradeoff in metallic glass cellular structures*, Acta Mater. 73 (2014) 259–274.
[34] K. Liu, R. Sun, C. Daraio, Growth rules for irregular architected materials with programmable properties, Science 377 (6609) (2022) 975–981.
[35] B. Yu, et al., The design of "Grain Boundary engineered" architected cellular materials: the role of 5-7 defects in hexagonal honeycombs, Acta Mater. 243 (2023) 118513.
[36] L. Xu, et al., Harnessing structural stochasticity in the computational discovery and design of microstructures, Mater. Des. 223 (2022) 111223.
[37] J.S. Zhang, et al., Stochastic or deterministic: duality of fatigue behaviour of 3D-printed meta-biomaterials, Mater. Des. 245 (2024) 113296.
[38] T. Mukhopadhyay, S. Adhikari, Stochastic mechanics of metamaterials, Compos. Struct. 162 (2017) 85–97.
[39] S. Yu, et al., Engineered disorder in photonics, Nat. Rev. Mater. 6 (3) (2021) 226–243.
[40] H. Zhu, J. Hobdell, A. Windle, Effects of cell irregularity on the elastic properties of 2D Voronoi honeycombs, J. Mech. Phys. Solids. 49 (4) (2001) 857–870.
[41] J. Alsayednoor, P. Harrison, Z. Guo, Large strain compressive response of 2-D periodic representative volume element for random foam microstructures, Mech. Mater. 66 (2013) 7–20.
[42] O.E. Sotomayor, H.V. Tippur, Role of cell regularity and relative density on elasto-plastic compression response of random honeycombs generated using Voronoi diagrams, Int. J. Solids. Struct. 51 (21–22) (2014) 3776–3786.
[43] N. Abid, M. Mirkhalaf, F. Barthelat, Discrete-element modeling of nacre-like materials: effects of random microstructures on strain localization and mechanical performance, J. Mech. Phys. Solids. 112 (2018) 385–402.
[44] Sotomayor, O., *Numerical modeling of random 2D and 3D structural foams using Voronoi diagrams: a study of cell regularity and compression response*. 2013.
[45] S. Choukir, et al., The interplay between constituent material and architectural disorder in bioinspired honeycomb structures, Int. J. Eng. Sci. 188 (2023) 103863.
[46] C. Chen, T. Lu, N. Fleck, Effect of imperfections on the yielding of two-dimensional foams, J. Mech. Phys. Solids. 47 (11) (1999) 2235–2272.
[47] Z. Zheng, J. Yu, J. Li, Dynamic crushing of 2D cellular structures: a finite element study, Int. J. Impact. Eng. 32 (1–4) (2005) 650–664.
[48] K. Li, X.-L. Gao, J. Wang, Dynamic crushing behavior of honeycomb structures with irregular cell shapes and non-uniform cell wall thickness, Int. J. Solids. Struct. 44 (14–15) (2007) 5003–5026.
[49] D.A. van Egmond, et al., The benefits of structural disorder in natural cellular solids, arXiv prepr (2021). arXiv:2110.04607.
[50] A. Ajdari, H. Nayeb-Hashemi, A. Vaziri, Dynamic crushing and energy absorption of regular, irregular and functionally graded cellular structures, Int. J. Solids. Struct. 48 (3–4) (2011) 506–516.
[51] N. Abid, J.W. Pro, F. Barthelat, Fracture mechanics of nacre-like materials using discrete-element models: effects of microstructure, interfaces and randomness, J. Mech. Phys. Solids. 124 (2019) 350–365.
[52] K. Karapiperis, D.M. Kochmann, Prediction and control of fracture paths in disordered architected materials using graph neural networks, Commun. Eng. 2 (1) (2023) 32.
[53] S. Choukir, N. Manohara, C.V. Singh, Disorder unlocks the strength-toughness trade-off in metamaterials, Appl. Mater. Today 42 (2025) 102579.
[54] I. Christodoulou, P. Tan, Crack initiation and fracture toughness of random Voronoi honeycombs, Eng. Fract. Mech. 104 (2013) 140–161.
[55] A. Montiel, et al., Effect of architecture disorder on the elastic response of two-dimensional lattice materials, Phys. Rev. e 106 (1) (2022) 015004.
[56] S. Luan, et al., A data-driven framework for structure-property correlation in ordered and disordered cellular metamaterials, Sci. Adv. 9 (41) (2023) eadi1453.
[57] T. Tancogne-Dejean, A.B. Spierings, D. Mohr, Additively-manufactured metallic micro-lattice materials for high specific energy absorption under static and dynamic loading, Acta Mater. 116 (2016) 14–28.
[58] L.J. Gibson, Cellular solids, Mrs. Bull. 28 (4) (2003) 270–274.
[59] H.S. Abdullahi, S. Gao, A novel multi-cell square tubal structure based on Voronoi tessellation for enhanced crashworthiness, Thin Walled Struct. 150 (2020) 106690.
[60] A. Kumar, et al., Energy absorption and stiffness of thin and thick-walled closed-cell 3D-printed structures fabricated from a hyperelastic soft polymer, Materials 15 (7) (2022) 2441.
[61] T. Wierzbicki, S. Bhat, A moving hinge solution for axisymmetric crushing of tubes, Int. J. Mech. Sci. 28 (3) (1986) 135–151.
[62] Wierzbicki, T. and W. Abramowicz, *On the crushing mechanics of thin-walled structures*. 1983.
[63] J. Hutchinson, Mechanisms of toughening in ceramics, Theor. Appl. Mech. (1989) 139–144.
[64] W.J. Clegg, et al., A simple way to make tough ceramics, Nature 347 (6292) (1990) 455–457.
[65] Z.C. Xia, et al., On large scale sliding in fiber-reinforced composites, J. Mech. Phys. Solids. 42 (7) (1994) 1139–1158.
[66] J. George, M.S. Sreekala, S. Thomas, A review on interface modification and characterization of natural fiber reinforced plastic composites, Polym. Eng. Sci. 41 (9) (2001) 1471–1485.
[67] J.Y. Sun, et al., Highly stretchable and tough hydrogels, Nature 489 (7414) (2012) 133–136.
[68] Y. Wang, et al., Highly ionic conductive, stretchable, and tough ionogel for flexible solid-State supercapacitor, Small (2023) 2307019.